**Advanced Steel Construction** – Vol. 20 No. 4 (2024) 330–344
**DOI:**10.18057/IJASC.2024.20.4.2


# STUDY OF MECHANICAL PROPERTIES OF A NOVEL COLUMN-BEAM-COLUMN PREFABRICATED STEEL FRAME JOINT

Zhi-Wei Zhang [1], Dong Li [2,*], Hua-Jie Wang [1,*], Hong-Liang Qian [1], Wen-Qi Fang [1], Xiao-Fei Jing [3] and Feng Fan [4]

[1] *Department of Civil Engineering, Harbin Institute of Technology at Weihai, Weihai 264209, China*
[2] *Weihai construction group Co., Ltd., Weihaig, China*
[3] *China State Construction first Bureau Co., Ltd., Beijing, China*
[4] *School of Civil Engineering, Harbin Institute of Technology, Harbin, China*
** (Corresponding author: E-mail: 40256724@qq.com; huajie_wang@hit.edu.cn)*

**ABSTRACT**

Currently, most research on prefabricated steel frame joints focuses on column-column or beam-column connections. However, there has been a lack of effective research on prefabricated column-beam-column joints with higher construction efficiency. In this paper, we present the construction and installation process and technical characteristics of a novel prefabricated column-beam-column joint (NPJ). Initially, we describe the technical specifications of the NPJ. Following this, we examine the mechanical performance of the NPJ using a validated finite element model and conduct a detailed analysis of various parameters affecting its performance. Subsequently, we propose a simplified method for calculating the performance of the NPJ, adhering to existing design codes. Our findings indicate that the NPJ exhibits robust mechanical properties, closely matching those of traditionally welded joints. Notably, the height of the beam emerges as a critical factor influencing the NPJ's load-bearing capacity, more so than the thickness of the lug. This research offers valuable insights and technical guidance for further exploration and practical application of prefabricated steel frame joints.

**ARTICLE HISTORY**

Received: 19 October 2023
Revised: 27 February 2024
Accepted: 4 March 2024

**KEYWORDS**

Prefabricated;
Column-beam-column joint;
Mechanical properties;
Finite element analysis;
Simplified calculation method



## 1. Introduction

Prefabricated steel structures, characterized by their components being manufactured in a factory setting prior to assembly on-site through bolting mechanisms, have garnered considerable interest in recent years. This heightened attention can be attributed to their notable advantages, including enhanced construction efficiency, consistent installation quality, and environmental sustainability [1]. Within these structures, joints play a pivotal role, bearing the brunt of complex forces [2,3]. Given the critical nature of these forces, it becomes imperative to pursue rigorous research focused on the joints within prefabricated steel structures.

Recent explorations into prefabricated steel joints for precast concrete structures have attracted considerable scholarly attention, evidenced by a series of investigations aiming to enhance structural resilience and efficiency [4,5]. Despite these advancements, the field's understanding is still evolving, with several studies identifying critical limitations.

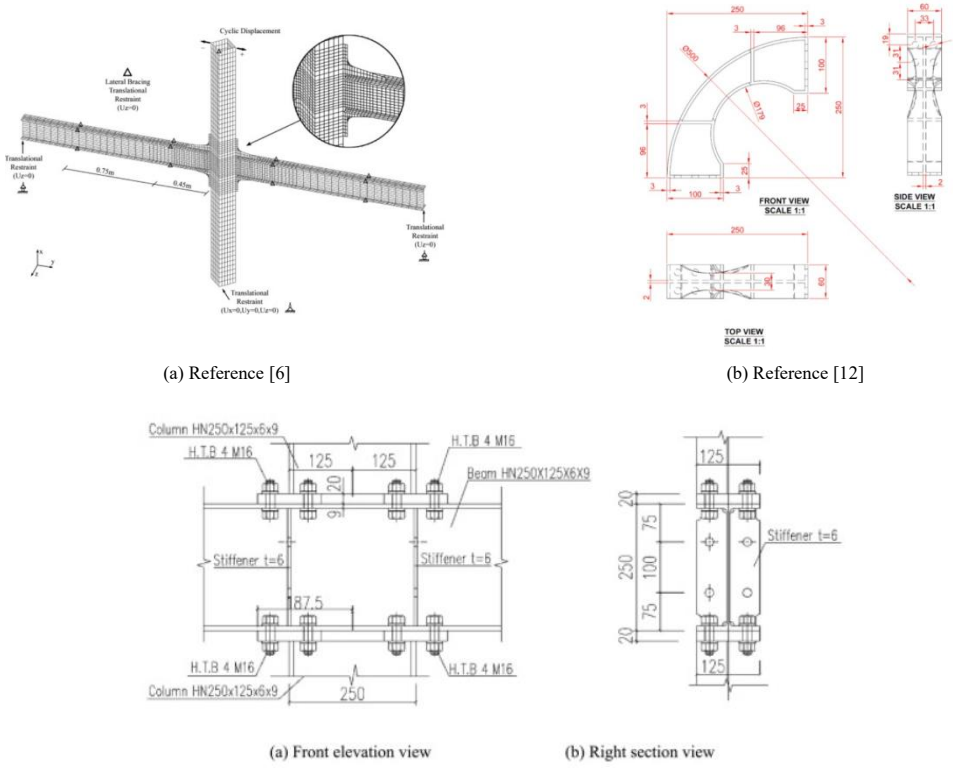


(a) Reference [6]

(b) Reference [12]

(a) Front elevation view

(b) Right section view

(c) Reference [15]

**Fig. 1** Prefabricated beam-column joints

Notably, Torabian et al. [6] introduced an innovative diagonal connection-type joint, which exhibited notable ductility in experimental settings. However, its complex design and unconventional approach to beam and column integration raised questions regarding its feasibility in standard construction practices [7]. Alternatively, Laiyun [8], Xiantie [9], and Zhouhong [10] presented a methodology for attaching the column to an end-plate via a

perforated split bolt, a technique demanding precise alignment of bolt holes, thus complicating its practical application. Further contributions by Jian et al. [11] entailed the development of a vertical connection node utilizing high-strength bolts, which, despite its innovative integration of a steel frame, pre-embedded edge steel frame, and steel casing, revealed that its seismic resilience requires enhancement. The incorporation of dampers into beam-column joints has been proven to significantly improve seismic performance [12-14], yet the high costs associated with this solution limit its widespread adoption. Hongkai et al. [15] proposed a moment-resisting joint designed for H-beam-columns, which demonstrated effective seismic capabilities in testing phases. However, the limited use of H-columns in practical engineering scenarios may restrict its applicability. The discourse has also extended to the replaceability of prefabricated beam-column joints post-earthquake [16-18], suggesting that positioning the connection near the column's end could facilitate easier replacement following seismic events [17, 19]. Regarding simplified calculations, there exists a consensus that most have been formulated in alignment with established design codes [20-22], underscoring a commitment to aligning innovative joint designs with regulatory standards and practical feasibility.

Recent studies on prefabricated frame joints have primarily concentrated on connections between beams and columns or between columns themselves. In contrast, the integrated column-beam-column joint offers a solution that addresses both vertical and horizontal connections within a steel frame structure using a single joint, significantly enhancing construction efficiency. Despite its potential, there has been limited effective research on these integrated joints [23], with existing studies narrowly focusing on specific mechanical properties [24], without a comprehensive overview.

To address these gaps, this research introduces a new type of prefabricated column-beam-column joint, named the novel prefabricated joint (NPJ). We detail the design, construction, and technical features of the NPJ. Following this, we developed and verified a detailed finite element model for the joint. Our investigation covers both static and seismic behaviors of the NPJs, comparing these properties to those of traditional welded joints. We also conducted parametric studies to understand how different geometric factors affect the NPJs' performance. Concluding our study, we propose simplified methods for estimating the load-bearing capacity and initial stiffness of NPJs, based on standard design code formulas. This work aims to serve as a useful resource for future research and practical applications of prefabricated steel frame joints.

## 2. Novel prefabricated joints

Building on existing prefabricated beam-column joint designs, the authors have made enhancements [24], creating an innovative joint that supports beams of varying heights. This joint is ingeniously constructed from four key prefabricated parts:

(1) **Lower Column**: Includes a flange end plate and a lug, the latter designed with an extension bolt hole for secure attachment.

(2) **Connector**: This piece links the H-shaped steel beam to the lower column's lug, ensuring a stable connection.

(3) **H-shaped Steel Beam**: Features an end plate for easy integration into the joint structure.

(4) **Upper Column**: Comes with a bolt hole and an upper column flange plate to complete the assembly.

The installation process is straightforward and efficient. It begins with attaching the lower connector to the column's lug plate using friction-type high-strength bolts. Next, the H-beam is positioned on top of the lower connector and secured with compression-type high-strength bolts. Finally, the beam is joined to the upper connector and lug plate with similar bolts, ensuring a firm assembly. This process, detailed in Fig. 2, showcases the methodical steps taken to assemble this advanced joint.

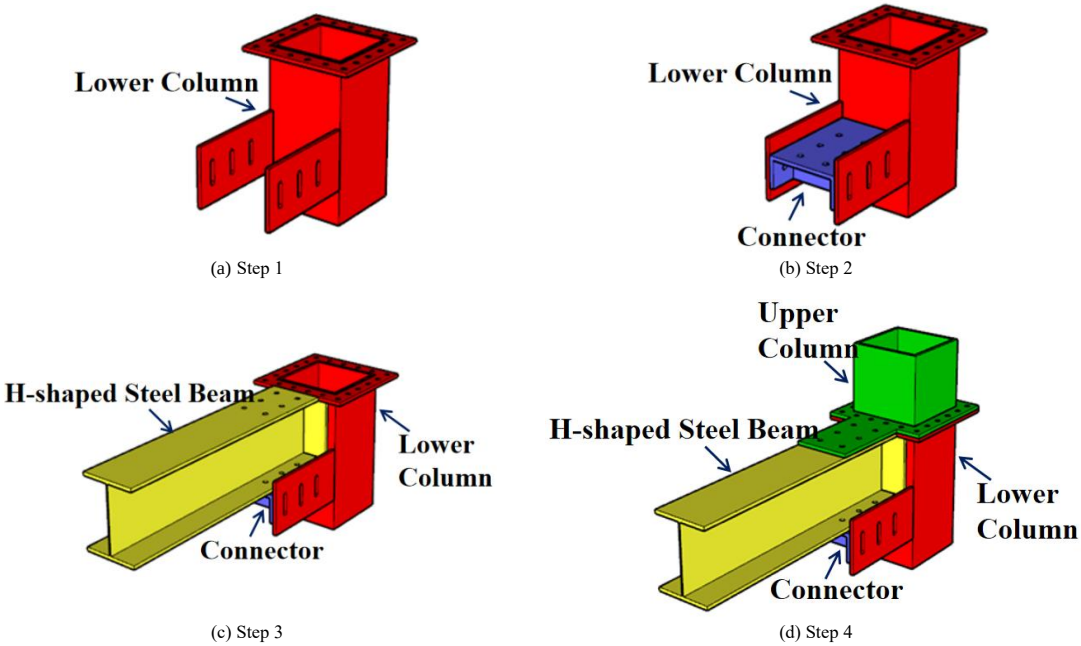


(a) Step 1 (b) Step 2

(c) Step 3 (d) Step 4

**Fig. 2** Composition of joints and installation process

The NPJs offer significant technical advantages compared to welded steel frame joints and other prefabricated beam-column joints:

(1) The construction process is straightforward. Both the column-to-column and column-to-beam connections are facilitated by a single joint, leading to a high level of prefabrication. The design also allows for the accommodation of H-shaped steel beams of varying section heights by adjusting the position of the lower connectors.

(2) The quality of construction is dependable. Components are pre-manufactured in a factory setting and assembled on-site using high-strength bolts, eliminating the inconsistencies associated with on-site welding.

(3) The path for force transfer is efficiently designed. The incorporation of lugs and lower connectors on the column enables shear force transfer while preventing the weakening of the column section that can occur with bolt holes. This ensures a reliable load transfer mechanism.

(4) Disassembly and replacement are made easy. Unlike other prefabricated joints, this innovative joint combines the column-to-column and column-to-beam connections at a single floor level. Its high level of prefabrication also allows for the selective replacement of beam and column components during maintenance or service.

## 3. Establishment and validation of the finite element model

Finite element analysis is a common method of studying the mechanical properties of steel members. In this study, the widely adopted finite element simulation software, ANSYS, was employed.

### *3.1. Joint dimensions and materials*

For a common three-story steel frame structure, one was chosen to numerically analyze the mechanical properties of the edge joints in the middle layer of the outer frame. The joint locations are depicted in Figure 3. Based on a typical joint cross-section, the column's cross-sectional dimensions were chosen to be 400*400*20 mm, and the beam's cross-section was selected as

H400*300*8*20 mm. The lug's connection to the joint employs high-strength friction-type bolts, while the remaining component connections utilize high-strength compression-type bolts. Fig. 4 shows the detailed dimensions of the joints.

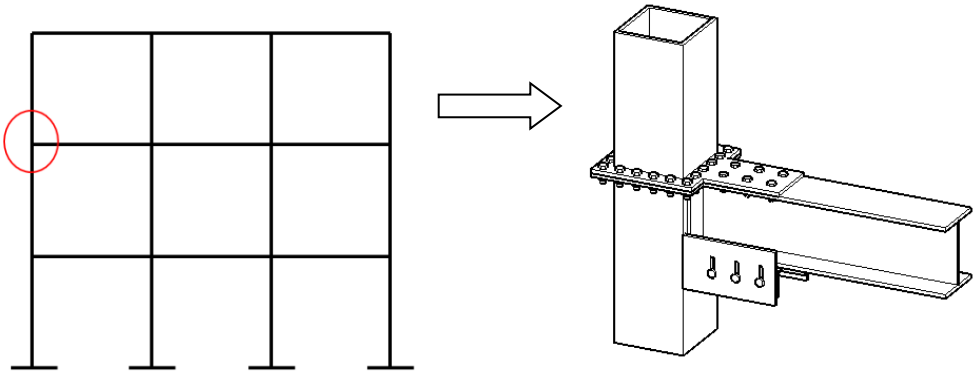

**Fig. 3** Location of the joint selection

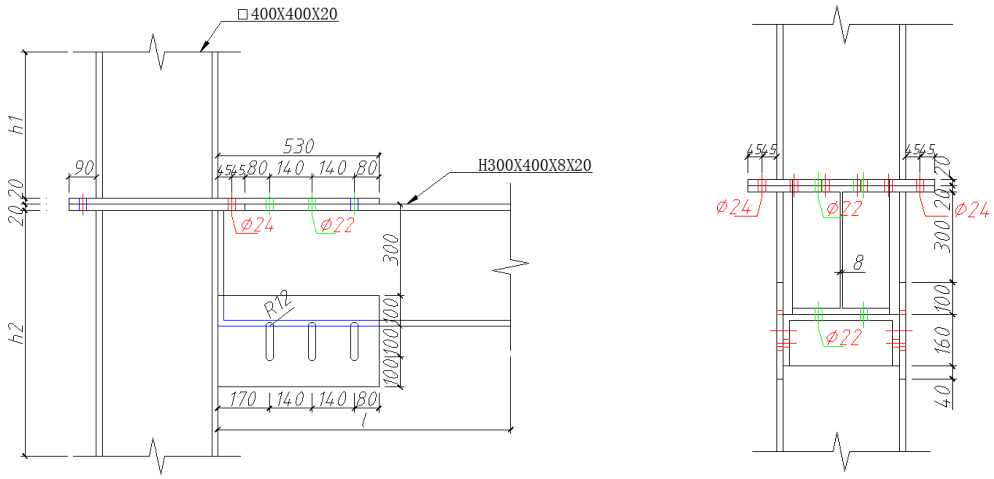


**Fig. 4** Dimensions of the joints (in mm)

**Table 1**
Material properties

| Material | Yield strength (MPa) | Ultimate strength(MPa) | Poisson ratio | Yield strain | Modulus of elasticity (GPa) | Tangential modulus (GPa) |
|---|---|---|---|---|---|---|
| Q355 steel | 345 | 500 | 0.3 | 0.167 | 206 | 4.12 |
| Grade 10.9 Bolt | 900 | 1000 | 0.3 | 0.437 | 206 | 4.12 |

The components of the typical joints are made of Q355 steel, and the bolts are all of grade 10.9. The property parameters of both materials are shown in Table 1.

*3.2. Finite element models*

To incorporate the steel's strengthening effect, the simulation utilized a bilinear follow-through strengthening criterion, with a bilinear model selected for the steel's stress-strain curve, as illustrated in Fig. 5. The joint was modeled using the SOLID 45 element, capable of simulating the plastic stress stiffening of steel. The model's elements were meshed using hexahedral mapping, with denser meshing in areas experiencing high stresses and complex stress patterns, as demonstrated in Fig. 6.

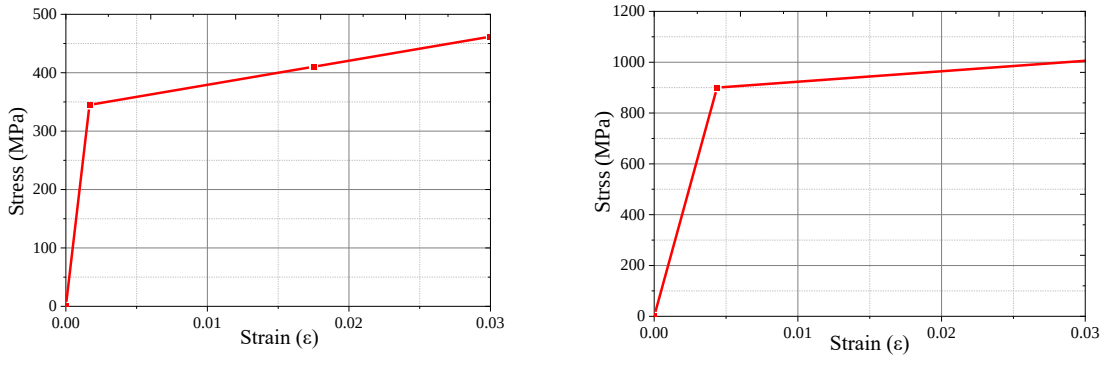


(a) Q345 steel

(b) Grade 10.9 bolt

**Fig. 5** Stress–strain curves of the materials

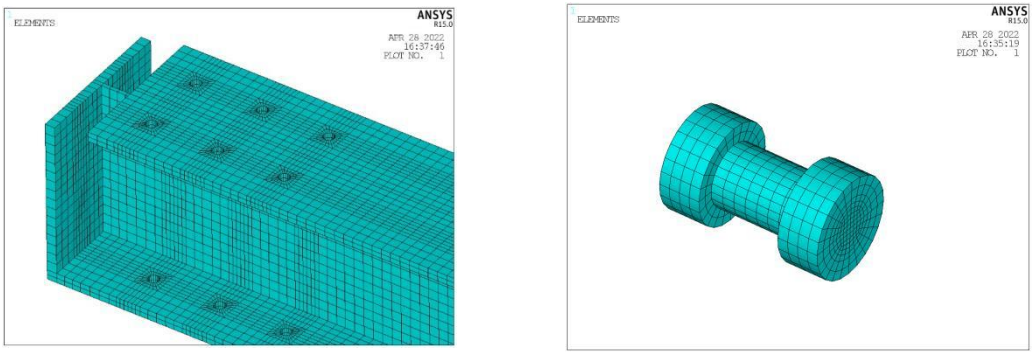


(a) Beam (b) Bolt

**Fig. 6** Meshing of the model

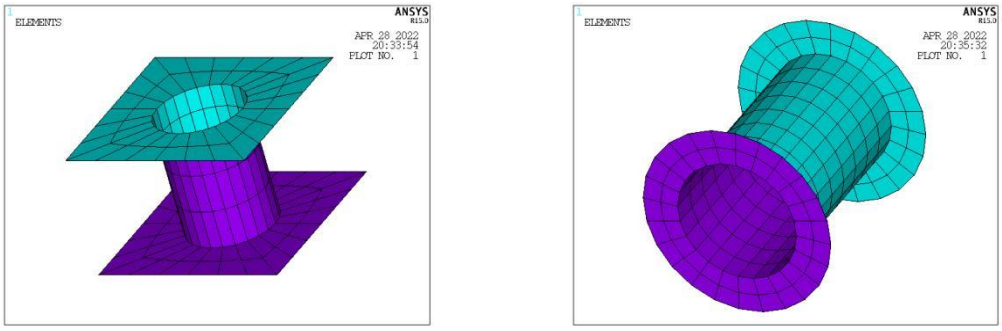


(a) CANTA174 elements (b) TARGE170 elements

**Fig. 7** Set-up of the contact elements in the bolt area

To enhance computational efficiency, the bolt shaft is represented as a cylinder, omitting the threads in the bolt modeling process. Given the high strength of the steel frame joints and minimal penetration during contact, CANTA174 and TARGE170 elements were chosen for the contact and target surfaces, respectively, as depicted in Fig.7. The rolled surfaces of each member were not specially processed, and a slip resistance factor of 0.35 was adopted, as referenced in the literature [11,19,25].

High tensile strength bolts are preloaded prior to installation using PRETS179 units. According to the steel design code [26], the preload force is set at 190 kN for M22 class 10.9 high-strength bolts and 225 kN for M24 high-strength bolts. Preload elements are positioned at the slab's contact surface. The joints' top and bottom column ends are fixedly restrained, and a downward displacement load is applied at the beam's end. The model's meshing employs the hexahedral mapping method preset in ANSYS finite element software, with the node model pre-divided to adhere to the hexahedral mapping delineation principle. Fig. 8 displays the comprehensive finite element model of the joint.

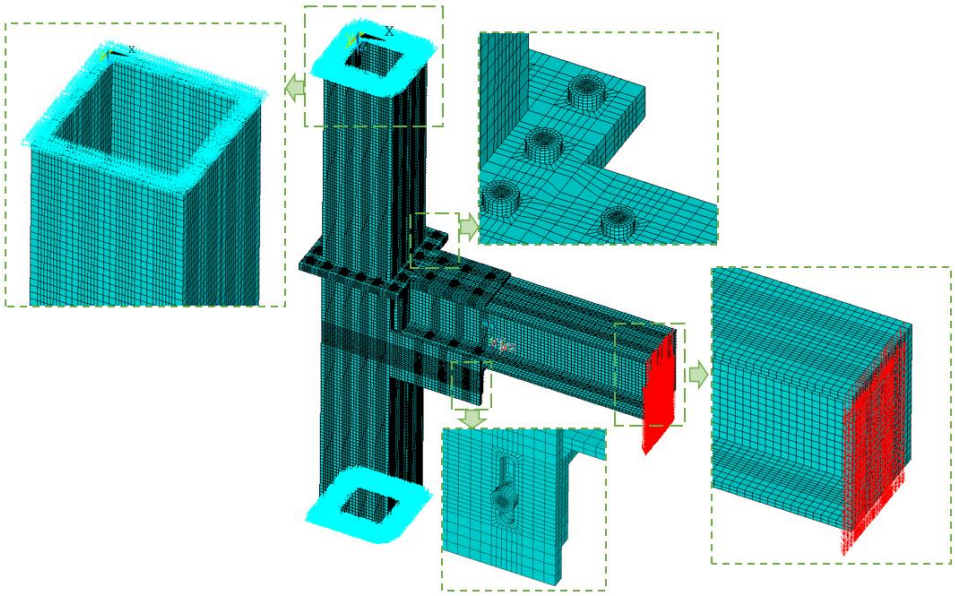

**Fig. 8** Overall finite element model

*3.3. Model validation*

To validate the appropriateness of the chosen setting parameters, a static load test [27] on a prefabricated beam-column joint, similar to the innovative joint introduced in this study, was selected for simulation and subsequent data comparison. Fig. 9 illustrates the experimental setup, where the column's bottom end is attached to a counterframe during the test, and the beam's left side is hinged to this counterframe. A vertical load is then applied to the beam's end using a jack. According to reference [27], the joint underwent detailed finite element modeling, with the established model showcased in Fig. 10.

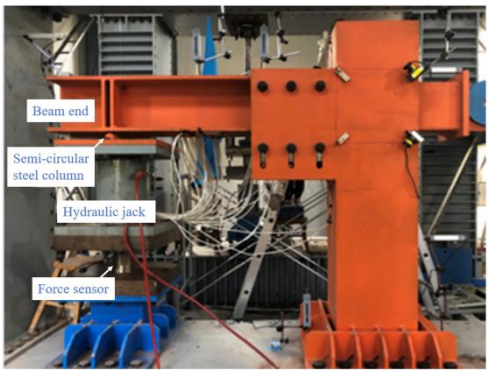


**Fig. 9** Test set-up

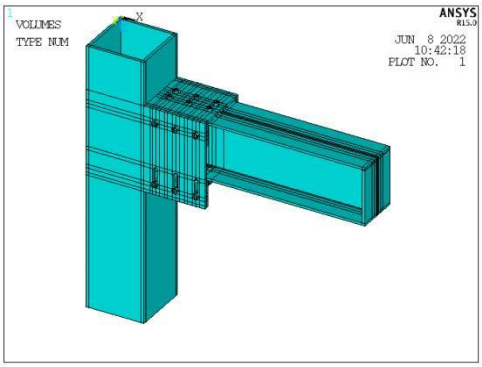


**Fig. 10** Finite element model of the joint

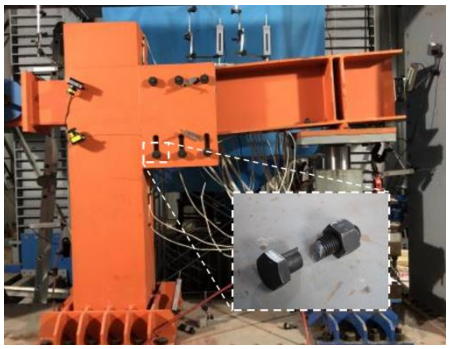

**Fig. 11** Ultimate state of the joint

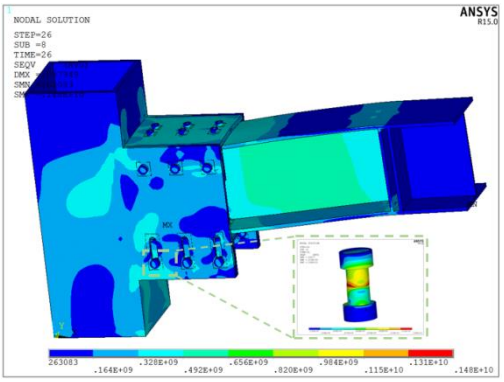


**Fig. 12** Stress nephogram

**Table 2**
Mechanical properties of the joint

| | Initial stiffness $K_1$ (MN·m/rad) | Ultimate bending moment Mu (kN·m) | Ultimate angle $\theta_u$ (rad) |
|---|---|---|---|
| FEM | 18.7 | 530.4 | 0.098 |
| Test[27] | 18.5 | 493.0 | 0.096 |

Fig. 11 displays the joint's ultimate state as observed in the experiment. Upon reaching the ultimate load, the beam noticeably displaces upward, with the primary mode of damage being tensile shear failure of the beam's lower flange bolts. The stress distribution, illustrated in Fig. 12 through a stress nephogram from the finite element analysis, closely aligns with the experimental outcomes. Notably, the simulation identified the maximum stress occurring at the lower flange bolt hole of the beam, peaking at 835 MPa, indicating bolt failure. This analysis confirms that the finite element model accurately captures the stress state and damage mode of the joint.

The mechanical properties analyzed for the joints in this study encompass stiffness, yield strength, ultimate strength, among others, as cited in references [27,28]. Table 2 presents a comparison of the mechanical properties derived from finite element simulations against experimental data. The close alignment between the finite element simulation outcomes and the experimental results demonstrates the accuracy of the FEM analysis in evaluating the performance of the joint.

## 4. Static performance

### *4.1. Mechanical response of NPJs*

The bending moment and rotation curve of the newly designed prefabricated joint (NPJ) under static load is depicted in Fig.13, revealing a distinct nonlinear segment that highlights the NPJ's substantial capacity for plastic deformation. Fig.14 illustrates the joint's stress state at failure, pinpointing high stress concentrations in the beam's web, at the interface between the upper column and the flange plate, and at the lower column's section contacting the beam. During joint failure, the stress in the column remains relatively low, not exceeding the material's yield strength. Significant stresses are noted at the connection between the upper column and the flange plate, and near the bottom edge of the lower column lug plate, though these do not lead to notable changes in the member's shape. The beam experiences high stress levels, with most of the web's stress exceeding the yield strength, leading to beam yielding and failure of some high-strength bolts.

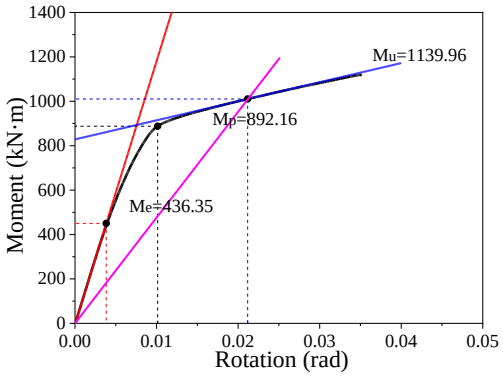


**Fig. 13** Bending moment and rotation curve

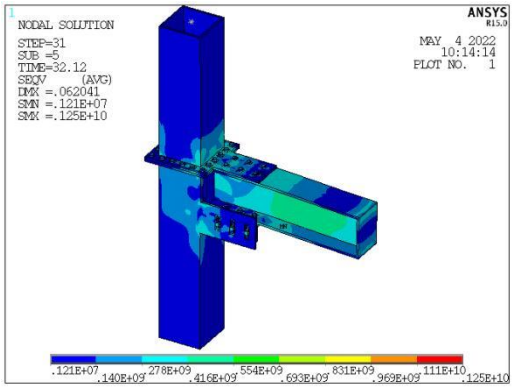


**Fig. 14** Stress nephogram at the ultimate condition

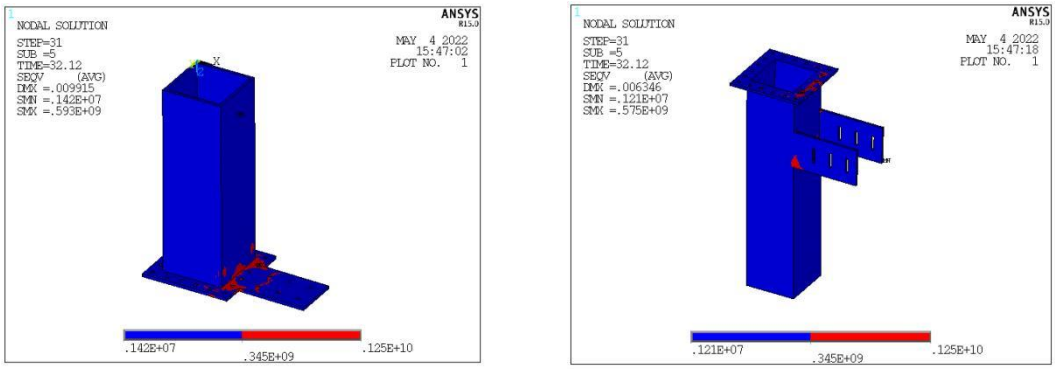


(a) Upper column (b) Lower column

**Fig. 15** plastic distribution of the columns at the ultimate condition

The depiction of plastic development in the joint at failure, shown in Fig.15, indicates that plasticity primarily occurs in the area where the flange plate connects to the column and around the first row of bolt holes close to the column. This is largely due to the significant bending moment at the upper column's end. Additionally, plasticity is observed at parts of the lower edge of the lug, mainly attributed to increased bending and shear forces at the edges and corners.

Fig.16 illustrates the stress state of the connector, with the maximum stress occurring at the edge of the beam's lower flange, reaching 417 MPa. The overall stress level of the connector remains within the elastic range. Fig.17 reveals that the high-strength bolts, which connect the column to the column, do not fail upon joint failure and maintain an elastic state. The stress levels in the high-strength bolts connecting the lower column to the connection are generally low, allowing the bolts to continue supporting the load effectively.

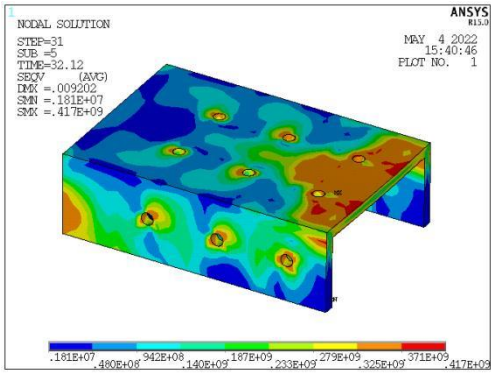


**Fig. 16** Stress nephogram of the connection

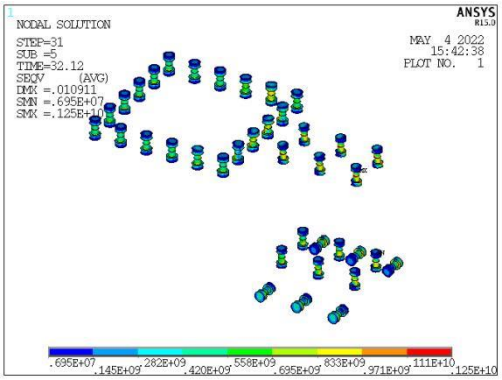


**Fig. 17** Stress nephogram of the bolts

**Table 3**
Mechanical properties of the two joints

| Joint | Elastic bending moment (kN·m) | Elastic turning angle (mrad) | Plastic bending moment (kN·m) | Plastic turning angle (mrad) | Ultimate bending moment (kN·m) | Ultimate turning angle (mrad) | Initial stiffness (kN·m/rad) | Strengthen stiffness (kN·m/rad) |
|---|---|---|---|---|---|---|---|---|
| Prefabricated | 436.4 | 4.3 | 892.2 | 11.4 | 1140.0 | 38.6 | 116757.6 | 8656.5 |
| Welded | 690.8 | 7.0 | 900.0 | 11.4 | 1312.2 | 189.6 | 100581.7 | 3832.0 |

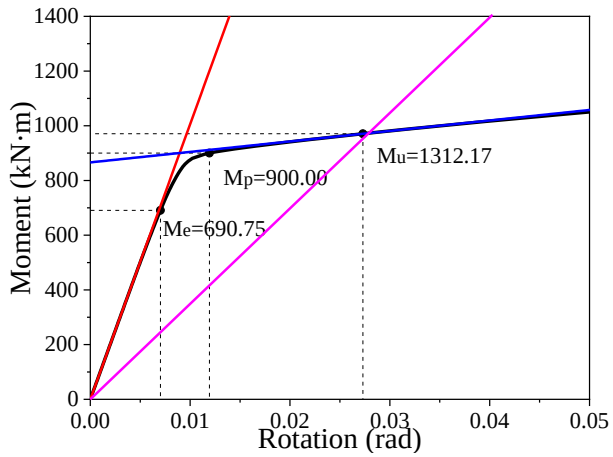


**Fig. 18** Bending moment and rotation curve of welded joint

*4.2. Comparison with the welded joint*

To compare the mechanical properties of the newly designed prefabricated joint (NPJ) with those of the traditional welded joint, a static load simulation was performed on both, using identical beam-column sizes. The comparison (Table 3) reveals that the NPJ's elastic bending moment is 58% higher than that of the welded joint, while the plastic bending moments are nearly identical, and the ultimate bending moment differs by 15.2%. When examining the plastic deformation capabilities of the two joints, it was found that the NPJ's elastic rotation angle is 38.8% smaller than that of the welded joint. However, the difference in ultimate bending moment between the two joints is minor, at approximately 13.2%.

When comparing the moment and rotation curves of the two types of joints, as illustrated in Fig.13 and 18, it becomes apparent that the novel prefabricated joint (NPJ) exhibits differences in deformation capacity primarily due to its larger initial and strengthening stiffness compared to the traditional welded joint. The design of the NPJ, with its connection method, provides increased stiffness at the column ends, resulting in minimal observable deformation.

The displacement nephogram (Fig.19) illustrates that the deformation of the NPJ's beam begins at the section protruding from the flange plate, whereas deformation in the welded joint is more pronounced at the beam-column connection. The damage to the welded joint results from bending and shear buckling of the beam. In contrast, damage to the NPJ primarily occurs through beam yielding, with damage extending to the ultimate state at the section of the beam's upper flange where the high-strength bolt is located. This comparison indicates that the static performance of the NPJ is comparable to that of the traditional welded joint, but with less displacement in the limit state and greater stiffness.

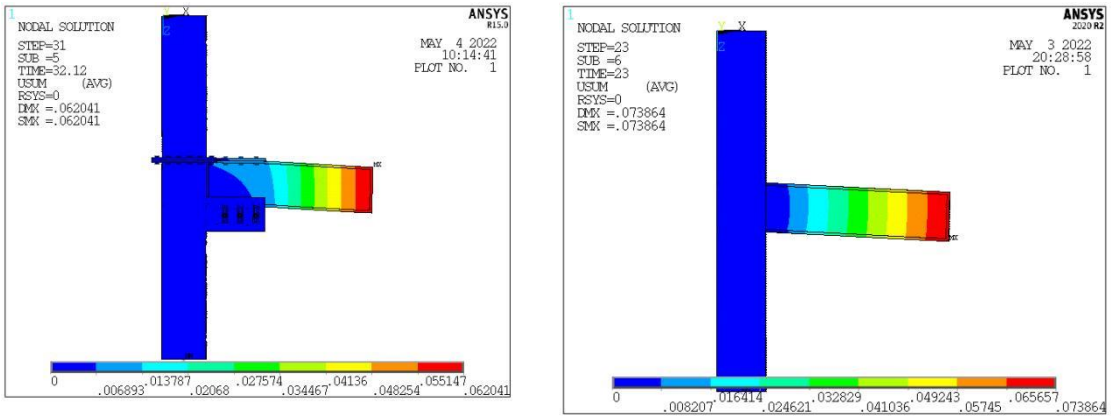


(a) Prefabricated joint (b) Welded joint

**Fig. 19** Displacement of the joints

## 5. Seismic performance

### *5.1. Hysteresis performance of NPJ*

The seismic performance of joints is assessed through displacement-controlled loading [26]. Once the joints achieve plastic displacement, the displacement load is incremented by 0.2 times the plastic displacement at each step, with each displacement level being applied for only one cycle. Upon reaching plastic displacement, the displacement at each subsequent level is doubled, and each level undergoes two cycles. Cyclic loading is discontinued when the member ceases to maintain its load-carrying capacity.

Fig.20 and 21 depict the stress and plastic distribution of the joint in its ultimate condition under hysteresis loading. The stress distribution in the column closely mirrors the results obtained under static loading, with the column predominantly remaining in the elastic phase. The maximum stress, at 343.48 MPa, is observed at the weld between the upper column and the flange plate. The web of the joint beam exhibits bulging and deformation, with both the upper and lower flanges and the web undergoing plastic deformation. The joint's failure mode is characterized by the beam yielding under bending and shear forces, exemplifying the principle of a strong column and weak beam.

The hysteretic and skeleton curves of the joint are presented in Fig.22 and 23. These figures highlight the joint's strong load-bearing capacity under both positive and negative bending moments. Initially, the joint operates within the elastic range, but as displacement increases, there is a noticeable decline in stiffness within a nonlinear segment. This leads to a reduction in the ultimate load capacity of the joint during the elasto-plastic phase, primarily attributed to bolt slippage. The fullness of the hysteretic curve underscores the joint's commendable seismic performance, indicating its resilience and reliability under seismic loading.

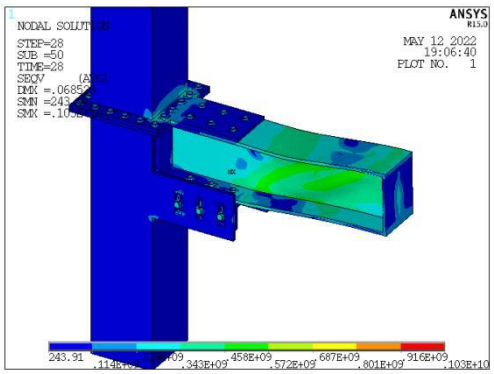


**Fig. 20** Stress nephogram under hysteretic loading

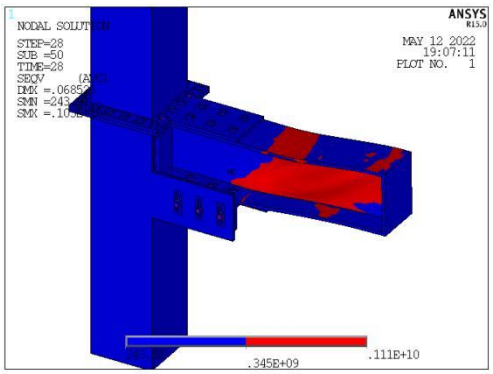


**Fig. 21** Plastic distribution under hysteretic loading

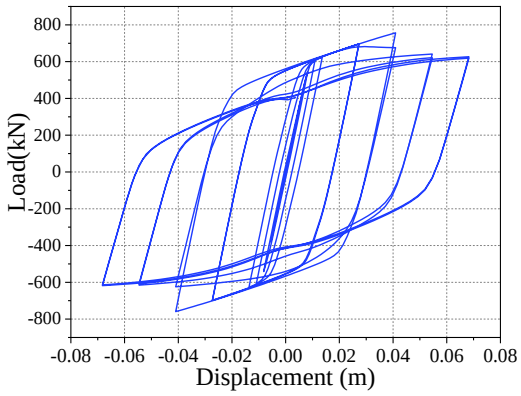


**Fig. 22** Hysteretic curve of NPJ

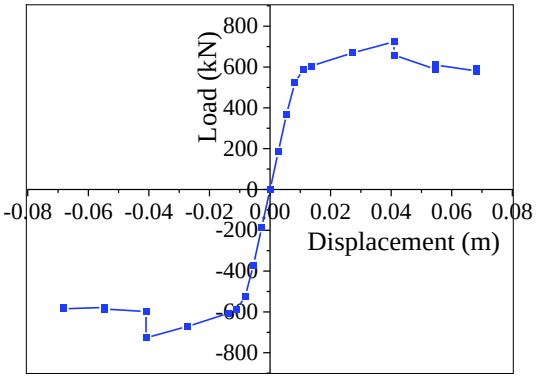


**Fig. 23** Skeleton curve of NPJ

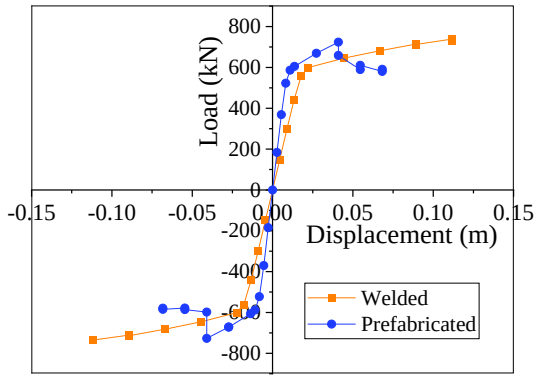


**Fig. 24** Comparison of skeleton curves

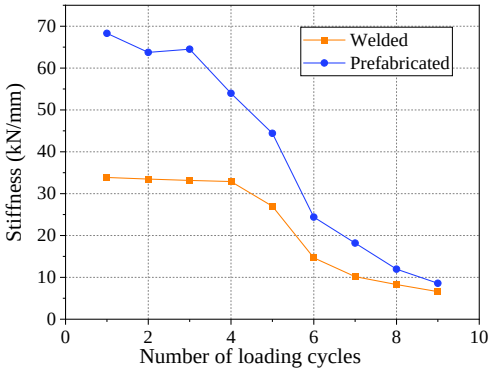


**Fig. 25** Comparison of stiffness degradation

*5.2. Comparison with the welded joint*

Fig.24 and 25 display the comparison of skeleton curves and stiffness degradation curves between different types of joints. The NPJs exhibit a superior maximum load capacity compared to traditional welded joints, albeit with a lesser deformation capability and greater initial stiffness. As loading cycles progress, NPJs experience a faster rate of stiffness reduction, but ultimately, the stiffness levels of both joint types converge to a similar point after undergoing stiffness degradation.

Table 4 presents the ductility coefficients and energy dissipation coefficients for the two types of joints. The ductility coefficient of the NPJs is lower than that of the traditional welded joints, which suggests that the NPJs have a marginally lower capacity for deformation compared to the welded joints. However, both types of joints have ductility coefficients greater than 4, demonstrating good ductility and energy dissipation capabilities. This performance aligns with the requirements of the seismic design code [26], indicating that both joint types are well-suited for seismic applications.

**Table 4**
Seismic behavior of two kinds of joints

| Joint | Ductility coefficient | Energy dissipation coefficient |
|---|---|---|
| Prefabricated | 8.32 | 3.72 |
| Welded | 6.07 | 3.46 |

## 6. Parametric analysis

*6.1. Parameter range in the investigation*

In this chapter, we analyze the geometric parameters of components that exhibit high stress levels during the failure of the joint to understand how changes in these parameters affect the static load mechanical properties and failure modes of the NPJs. Utilizing the previously described finite element model, the parameters under investigation include the flange thickness (FT) of the upper column, the number of bolts without altering the overall load-bearing capacity (BN), the lug thickness (LT) of the lower column, and the height of the H-shaped steel beam (BH). The models are named according to the convention FT-N, BN-N, LT-N, and BH-N, where "N" represents the value of the parameter. For instance, FT-16 denotes a model with a flange thickness of 16 mm, with all other geometric parameters remaining as described in Chapter 3. Details of each model are summarized in Table 5.

*6.2. The flange thickness (FT) of the upper column*

As previously discussed, the upper column's flange plate is subjected to shear and tensile forces resulting from the bending moment load, with its bearing capacity significantly influencing the joint's failure mode and mechanical properties. This section examines upper columns featuring flange thicknesses ranging from 12 mm to 28 mm.

Fig.26 illustrates the plastic nephograms of the joints as the flange thickness varies. When the flange plate's thickness is below 18 mm, the bolt hole area connecting the flange plate to the beam undergoes extensive plastic deformation, leading to a tensile failure mode of the flange plate. As the thickness increases, the extent of plastic deformation in the flange plate diminishes. Beyond a thickness of 22 mm, the flange plate remains in an elastic state under ultimate conditions, with a notable reduction in the plastic area around the bolt holes.

**Table 5**
Models in parametric analysis

| Parameters | Model number | Parameters information |
|---|---|---|
| Flange thickness | FT-(12/14/16/18/20/22/24/26/28) | Thickness: 12/14/16/18/20/22/24/26/28 mm |
| Number of bolts | BN-(10/8/6/4) | Number: 10/8/6/4 |
| Lug thickness | LT-(12/14/16/18/20/22/24/26/28) | Thickness: 12/14/16/18/20/22/24/26/28 mm |
| Height of the beam | BH-(340/350/360/370/380/400/420/440) | Height: 340/350/360/370/380/400/420/440 mm |

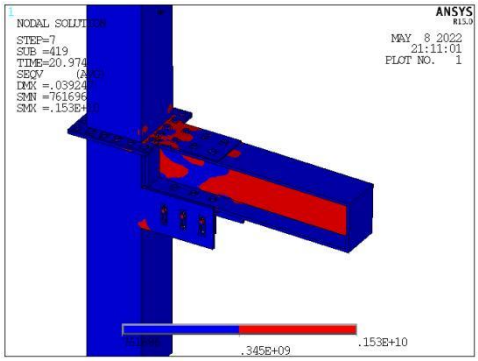


(a) FT-12

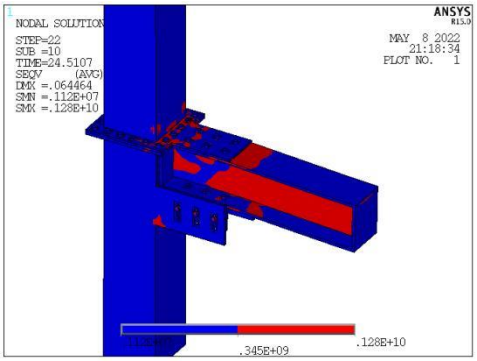


(b) FT-16

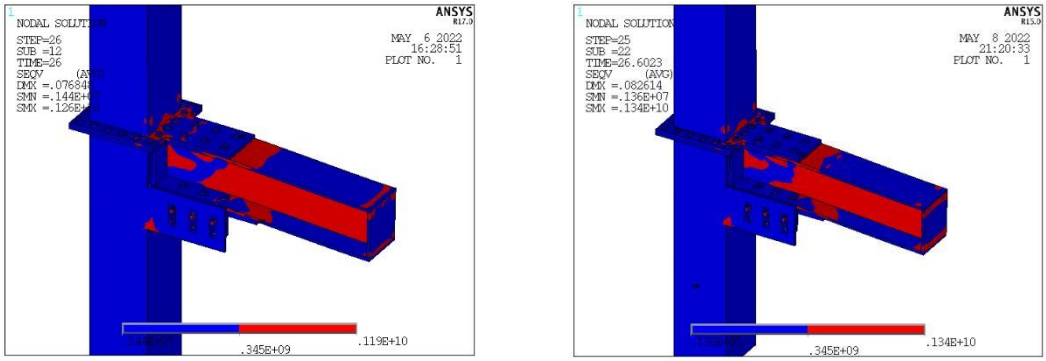


(c) FT-20 (d) FT-24

**Fig. 26** Plasticity nephograms with different FT

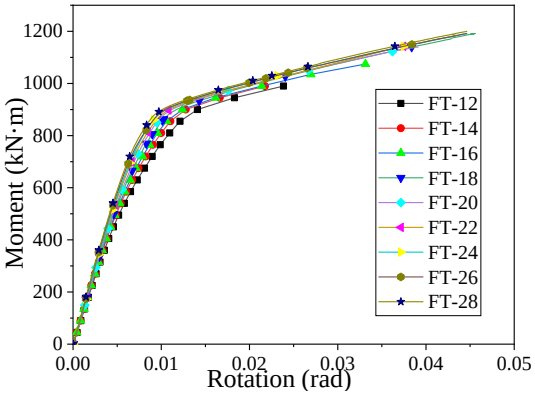


(a) Moment rotation curves

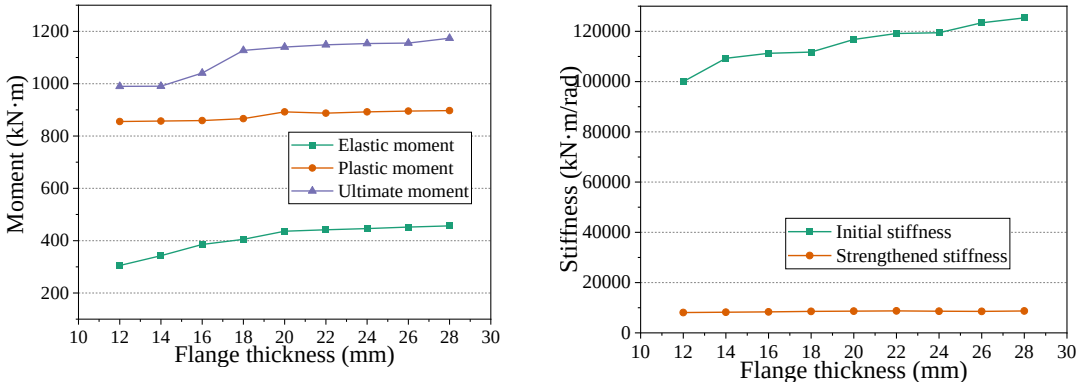


(b) Bearing capacity (c) Stiffness

**Fig. 27** Joints with different FT

Fig.27 presents the moment-rotation curves and mechanical properties of joints with varying flange thicknesses (FT). For FT values less than 18 mm, both the elastic and ultimate moments of the joints show an increase with the thickness. However, once the FT exceeds 18 mm, further increases in thickness have a minimal impact on the joints' load-bearing capacity. A thicker flange plate results in higher initial stiffness for the joint, though the enhancement in strengthening stiffness is relatively minor. With thinner flange plates, significant plastic deformation is evident in the ultimate condition, and the joint's elastic moment rises with the stiffness of the flange plate. When the flange plate's thickness is above 18 mm, it remains in the elastic phase under ultimate conditions, and failure is primarily governed by the bolt strength and the beam's load-bearing capacity, leading to little variation in the ultimate bending moment.

*6.3. Number of bolts (BN)*

The examination of different numbers and diameters of bolts on the beam's flange, as presented in the models (4*M27, 6*M22, 8*M20, and 10*M16), reveals a crucial insight into the joint's failure mechanics. Despite variations in the bolt arrangements, with total load capacities ranging from 405.1 kN to 502.2 kN, Fig.28 illustrates that the overall plastic distribution of the joint in its ultimate state remains largely unchanged across different bolt configurations. This consistency suggests that within the tested range, the number of bolts does not significantly influence the stress distribution and the development of plasticity within the joint. Consequently, the failure mode of the joints under ultimate load conditions appears to be relatively insensitive to variations in the number and size of the flange bolts, assuming their total load-bearing capacity is maintained within a comparable range.

Fig.29 reveals that the number of bolts (BN) has minimal impact on joint mechanical properties. However, using 4 × M27 bolts results in lower ultimate bearing capacity due to bending failure from insufficient bolts.

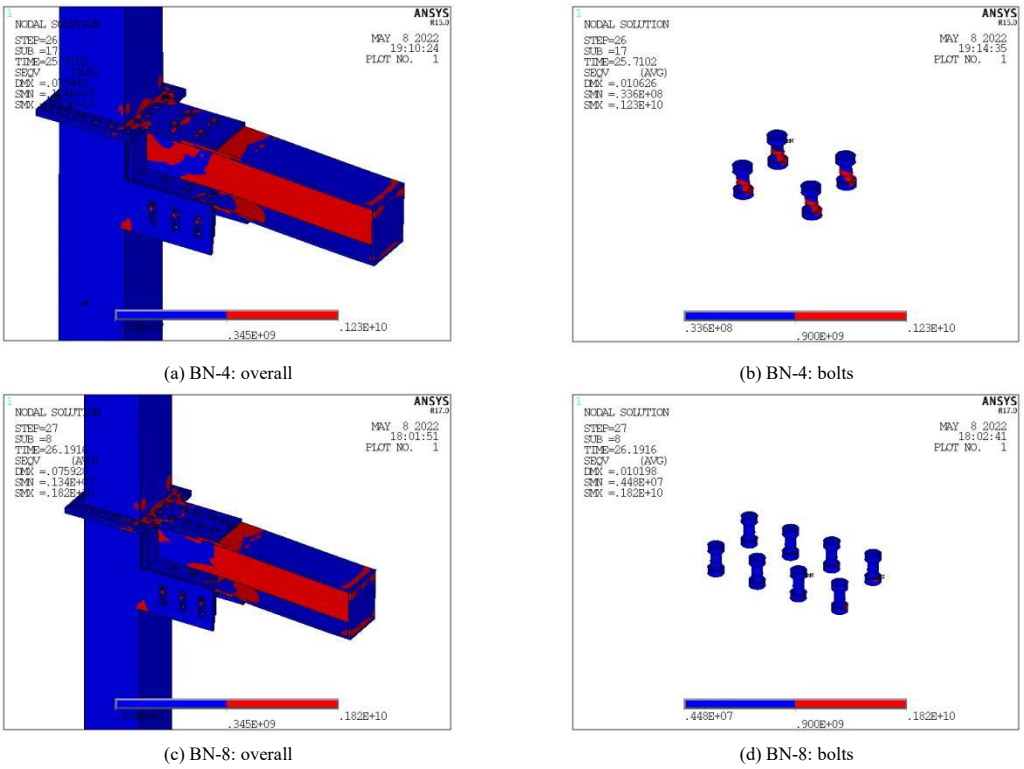


(a) BN-4: overall

(b) BN-4: bolts

(c) BN-8: overall

(d) BN-8: bolts

**Fig. 28** Plasticity nephograms with different BN

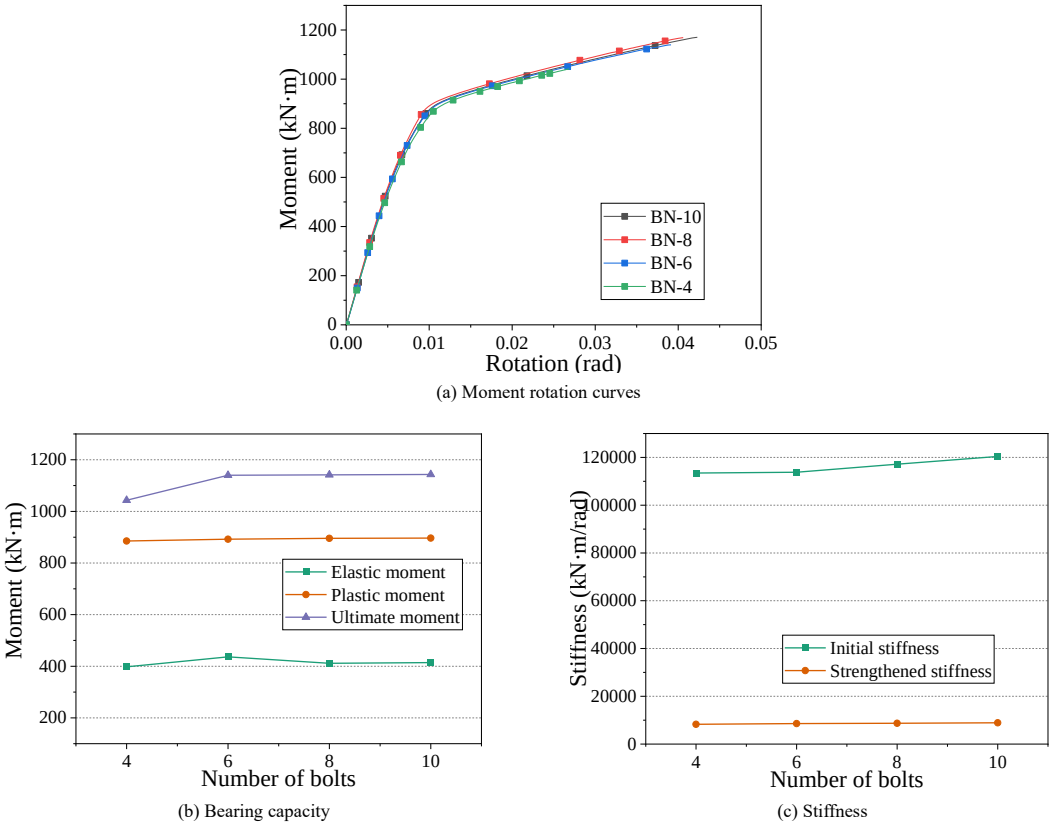


(a) Moment rotation curves

(b) Bearing capacity

(c) Stiffness

**Fig. 29** Joints with different BN

*6.4. Lug thickness (LT)*

The analysis of the lug's thickness (LT) in the lower column, ranging from 12 mm to 28 mm, shows its significant impact on the joint's stiffness and failure mode. Fig.30 illustrates the plastic deformation patterns for joints with varying LTs. With an LT of 12 mm, a noticeable plastic region is observed at the top and bottom edges of the lug near the column end, leading to damage through bending shear yielding of the beam. As the LT increases, the plastic deformation area of the lug steadily decreases. When the LT reaches 28 mm, the lug remains elastic, not undergoing plastic deformation, even when the joint is damaged. This indicates that increasing the LT enhances the lug's resistance to plastic deformation, potentially improving the joint's overall stiffness and altering its failure mode.

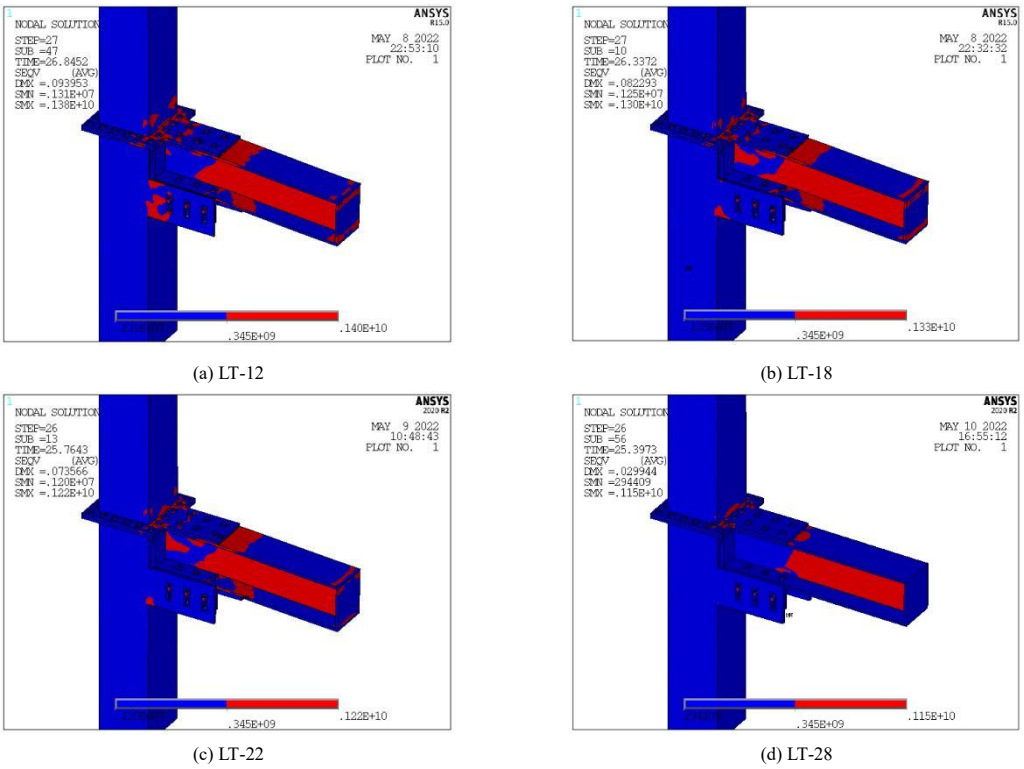


(a) LT-12 (b) LT-18

(c) LT-22 (d) LT-28

**Fig. 30** Plasticity nephograms with different LT

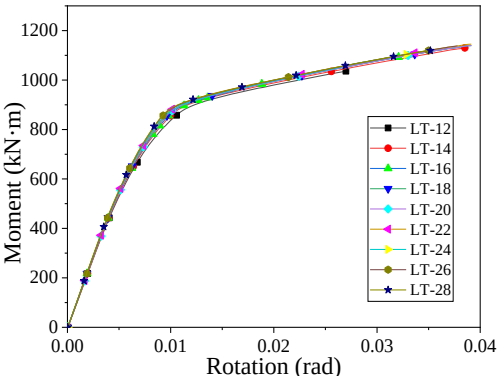


(a) Moment rotation curves

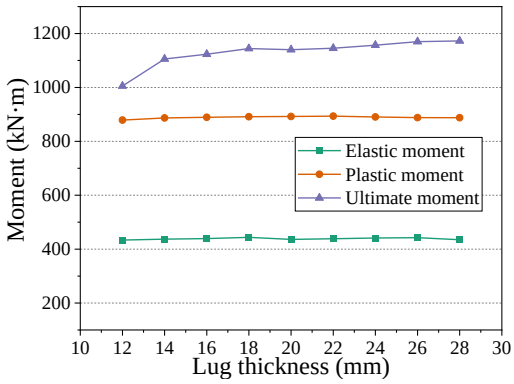


(b) Bearing capacity

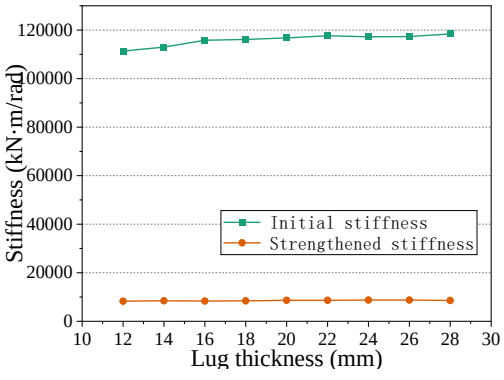


(c) Stiffness

**Fig. 31** Joints with different LT

The moment-rotation curves and mechanical properties of joints with varying lug thicknesses (LTs) highlight the influence of LT on joint performance, as depicted in Fig.31. While joints across different LTs maintain commendable plasticity, the augmentation of LT notably enhances the joint's elastic moment capacity, albeit without significantly impacting the plastic or ultimate moment capacities. This slight improvement in initial stiffness attributed to increased LT suggests that while the lug possesses considerable stiffness, its modification has minimal impact on the overall mechanical properties and failure mode of the joint. This observation implies that the advantages gained from increasing the LT are marginal, indicating that other design or reinforcement strategies may be more effective for significantly enhancing joint performance.

### *6.5. The height of the beam (BH)*

The influence of the beam height on the plastic deformation and failure mode of the joint is significant, as illustrated in Fig.32. This variation in beam height from 340 mm to 440 mm notably affects the joint's semi-rigid performance and its failure mechanism. Initially, at a beam height of 340 mm, both the beam flange and the web near the column end undergo extensive plastic deformation, indicating fully developed plasticity within the joint. The primary failure mode here is the yielding of both the beam and flange plate,

suggesting a balanced distribution of plastic zones across critical areas of the joint.

As the beam height increases, there is a consistent reduction in the plastic zones on the upper column flange plate and the connection between the beam and column. This reduction alters the failure mode of the joint. At a beam height of 380 mm, the connection's plastic zone vanishes, shifting the failure mode towards bending and shear yield of the beam, coupled with the failure of some high-strength bolts on the beam. This change indicates a transition from a more distributed plastic deformation towards localized failure points, reflecting the impact of beam height on joint performance.

Upon reaching a beam height of 440 mm, the failure mode further evolves, with only the web area of the beam entering plasticity, leading to the compression failure of high-strength bolts on the beam. This progression demonstrates a significant shift in the joint's failure mechanism, from a more distributed plastic deformation across multiple components to a localized failure primarily within the beam's web and associated bolt failures. This highlights the critical role of beam height in determining the structural behavior and resilience of the joint under load, emphasizing the need for careful consideration of beam dimensions in joint design to optimize performance and failure response.

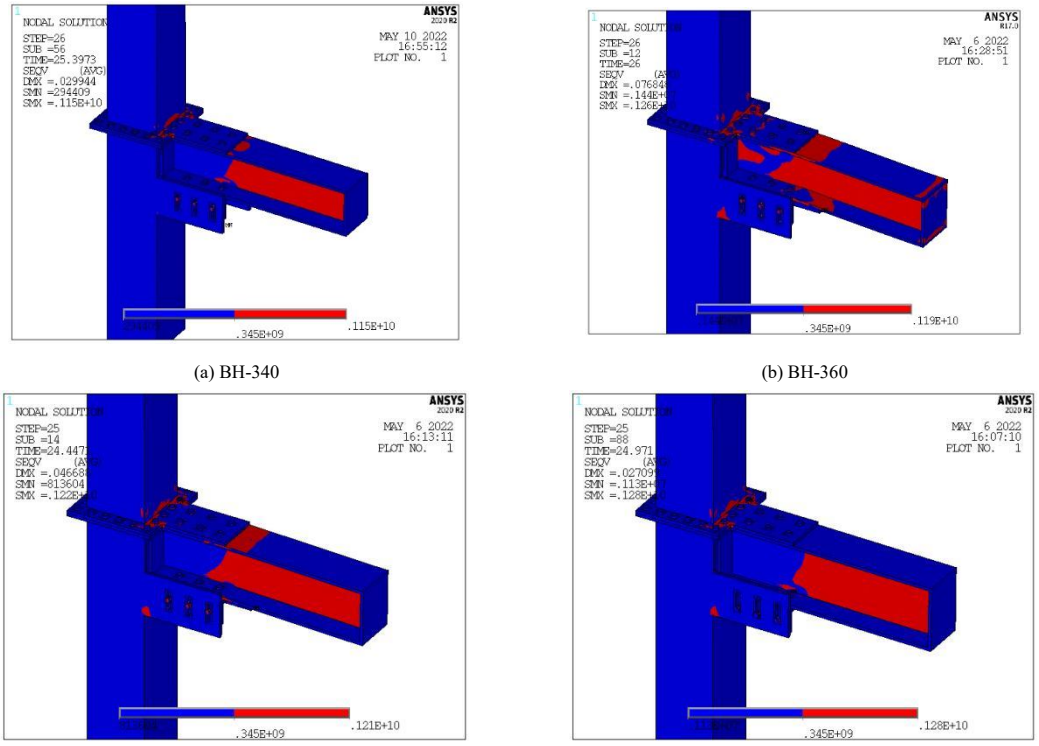


(a) BH-340 (b) BH-360

(c) BH-380 (d) BH-440

**Fig. 32** Plasticity nephograms with different BH

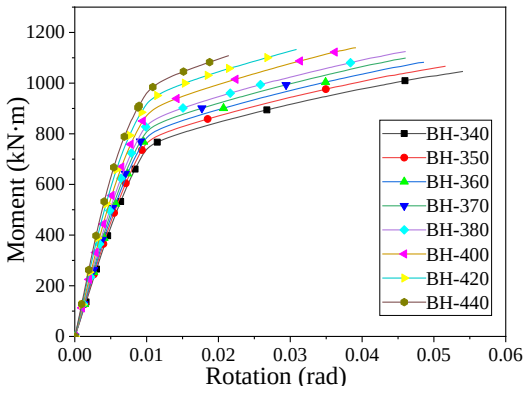


(a) Moment rotation curves

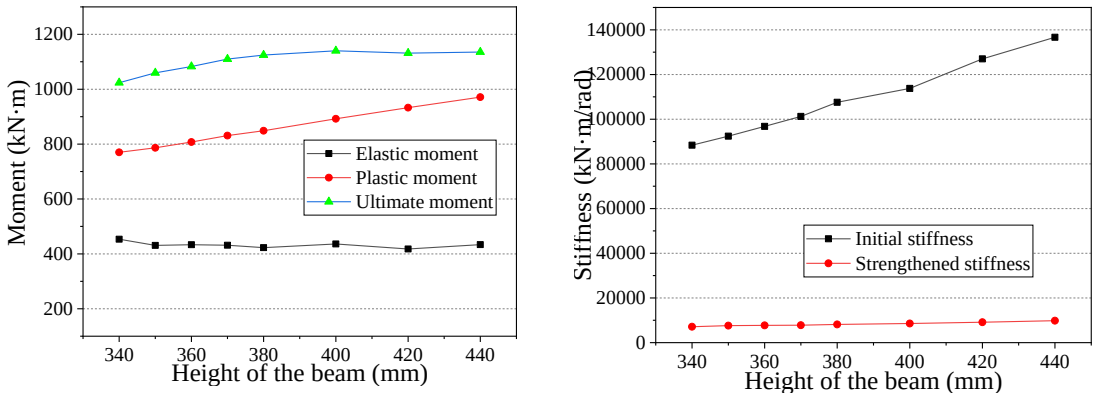


(b) Bearing capacity (c) Stiffness

**Fig. 33** Joints with different BH

The analysis of joints with different beam heights (BH) in Fig.33 shows that beam height significantly affects the joint's initial stiffness and deformation capacity. Higher beam heights increase initial stiffness but reduce rotation capacity. This indicates the stiffness of the beam plays a critical role in the joint's overall stiffness, which increases with beam height. Lower beam heights allow for greater beam deformation, influenced by the upper column flange, leading to plastic deformation in both the beam and the flange plate. As beam height increases, the deformation and plastic rotation capacity decrease, altering the failure mode. This suggests lower beam heights optimize the joint's performance by maximizing the plastic capacity of both the upper column flange plate and the beam, highlighting the importance of beam dimensions in joint design for structural integrity and performance.

## 7. Simplified calculation method

Previous research demonstrated that Nonlinear Plastic Joints (NPJs) exhibit robust load-bearing capacity and stiffness. This section evaluates the NPJs' load-bearing capabilities and stiffness in accordance with two prevalent design standards, GB50017 [26] and Eurocode3 [29]. The aim is to support the design and practical application of NPJs more effectively.

### *7.1. Calculation of load bearing capacity based on GB50017*

Currently, there's no standard calculation method for prefabricated joints. This paper calculates the load capacity of each component based on the joints' force transfer mechanism. As illustrated in Fig. 34, the joint area is subject to the beam's bending moment and shear force. Extensive research [7, 11-13, 19, 22] indicates that adhering to the design philosophy of ensuring joints are stronger than adjoining members, joints fail due to the bending-shear buckling of beams, with other components not reaching their maximum load capacity at failure. The stress distribution in the beam at failure can be simplified to the entire section yielding, with the peak stress reaching the material's tensile strength, as depicted in Fig. 35.

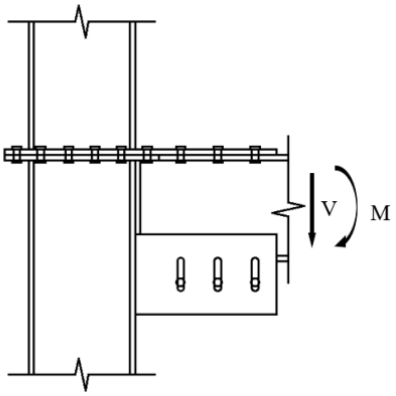


**Fig. 34** Force transfer at the end of the beam

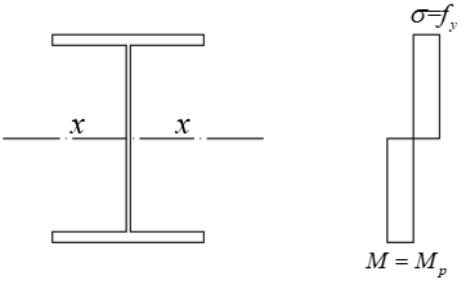


**Fig. 35** Maximum stress distribution of beam section

Because the beam section is subjected to the combined action of bending moment and shear, the ultimate bearing capacity of joint beam members can be determined as min {Vum,Vuv,V1}, where Vum is the ultimate bearing capacity under bending moment, Vuv is the ultimate bearing capacity under shear, and V1 is the ultimate bearing capacity under the combined action of bending moment and shear. The calculation methods of the three kinds of bearing capacity are as follows:

(1) Ultimate bearing capacity under bending moment

Considering the plastic capacity of the joint web, the maximum bending moment of the beam member is Meu= Vum*L, so the bearing capacity Vum under the bending moment can be calculated by equation (1):

$$V_{um} = \gamma_x \alpha_e W_x f / L \tag{1}$$

where γx is the plastic development coefficient of the section, Wx is the modulus of the section around the x-axis, f is the design value of the tensile strength of the steel, and αe is the reduction coefficient of the beam considering the effective height of the web.

(2) Ultimate bearing capacity under shear

The general width-thickness ratio λs of joints can be calculated by equation (2):

$$\lambda_s = \frac{h_0 / t_w}{41\sqrt{5.34 + 4\left(h_0 / a\right)^2}} \sqrt{\frac{f_y}{235}} \tag{2}$$

where Ix is the moment of inertia of the web section around the x-axis, hc is the height of the web in compression calculated for the full section, tw is the design value of the tensile strength of the steel and ρ is the effective height factor of the web under compression.

The general width-thickness ratio λs for different beam height joints is found to be less than 0.8. The maximum shear value Vuv, taking into account the plastic capacity of the joint web, can be calculated using equation (3):

$$V_{uv} = h_w t_w f_v \tag{3}$$

where hw is the height of the beam web, fv is the design value of the shear strength of the steel and tw is the thickness of the beam web.

(3) Ultimate bearing capacity under the combined action of bending moment and shear

As mentioned before, the dangerous section of the beam is the edge section of the beam protruding from the flange plate of the upper column. The dangerous section bears a large bending moment and shear force, and the combined action of the bending moment and shear force should be used to calculate the beam when designing the joint. Because the bending moment of the beam does not exceed the bending capacity of the upper and lower flanges Mf, the shear capacity of the beam is still Vuv, and the shear force V1 at the end of the beam should satisfy equation (4):

$$\left(\frac{V_1}{0.5V_{uv}} - 1\right)^2 + \frac{V_1 \bullet L - M_f}{V_{um} \bullet L - M_f} \le 1 \tag{4}$$

The ultimate bearing capacity of joints under different beam heights is calculated by the above equations, as shown in Table 6. The ultimate bearing capacity of joints calculated by the simplified calculation method is 60% and 80% of the finite element simulation results. The above differences are mainly because the design value of the shear strength of the material is considered to be 58% of the tensile strength in the code[26] for safety reasons. Generally, the cross-section size of the NPJs can be designed by design code GB50017, and the designed joint has a large safety reserve.

**Table 6**
Ultimate bending bearing capacity of joints

| Geometrical parameters | Finite element method (kN) | Simplified calculation method (kN) | Result difference (%) |
|---|---|---|---|
| BH340 mm | 682.32 | 432 | 63.31 |
| BH350 mm | 706.36 | 446.4 | 63.20 |
| BH360 mm | 721.75 | 460.8 | 63.84 |
| BH370 mm | 739.97 | 475.2 | 64.22 |
| BH380 mm | 749.70 | 489.6 | 65.31 |
| BH400 mm | 759.97 | 518.4 | 68.21 |
| BH420 mm | 754.41 | 547.2 | 72.53 |
| BH440 mm | 757.02 | 576 | 76.09 |

### *7.2. Calculation of initial stiffness based on GB50017*

To evaluate the deformation capacity of joints, the initial stiffness of joints was calculated by using the code Eurocode3. As shown in Fig. 36, the initial stiffness of a beam-column joint with bolts is a combination of shear column web stiffness $k_1$, compression column web stiffness $k_2$, tension column web stiffness $k_3$, bending flange splint stiffness $k_6$ and shear bolt stiffness $k_{11}$. The stiffness of the joints can be calculated by equation (5) as

$$S_j = \frac{Ez^2}{\mu \sum_i \frac{1}{k_i}} \tag{5}$$

Ki is the stiffness of the basic joint components, z is the rotating arm, that is, the beam height of the H-shaped steel beam, E is the elastic modulus of steel, and μ is the joint stiffness ratio, taken as 1.0.

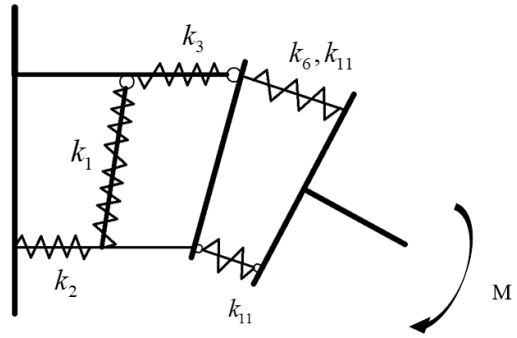


**Fig. 36** Calculation of initial stiffness

The shear column web stiffness $k_1$ can be calculated according to equation (6).

$$k_1 = \frac{0.38 A_{VC}}{\beta z} \tag{6}$$

where $A_{vc}$ is the shear area of the square steel tube column, $\beta$ is the transformation parameter, taken as 1.0, and $z$ is the shear force arm, taken as the height from the upper flange to the bolt hole in the lug.

The compression column web stiffness $k_2$ can be calculated according to equation (7).

$$k_2 = \frac{0.7 b_{eff,t,wc} t_{wc}}{d_c} \tag{7}$$

where $b_{eff,t,wc}$ is the effective width of the compressed column web, $t_{wc}$ is the thickness of the compressed column web and dc is the height of the compressed column web.

The tension column web stiffness $k_3$ can be calculated according to equation (8).

$$k_3 = \frac{0.7 b_{eff,t,wc} t_{wc}}{d_c} \tag{8}$$

where $b_{eff,t,wc}$ is the effective width of the tensioned column web, $t_{wc}$ is the thickness of the tensioned column web and dc is the height of the tensioned column web.

The bending flange splint stiffness $k_6$ can be calculated according to equation (9).

$$k_6 = \frac{0.9 \ell_{eff} t_a^3}{m^3} \tag{9}$$

where $l_{eff}$ is the effective thickness of the flange, taken as 1/2 of the flange plate width, $t_a$ can be taken as the flange plate thickness, and m is the sum of the joint flange plate thickness and the column flange thickness.

Due to the use of friction-type high-strength bolts, the shear bolt stiffness $k_{11} = \infty$.

To verify the rationality of the simplified calculation method, finite element analysis and theoretical values were calculated for the NPJs with different geometrical dimensions, the results of which are compared in Fig. 37. It can be found that the initial stiffness of the theoretical calculation is slightly higher than the stiffness of the simulation result, and the difference between the two is less than 10%. It is worth mentioning that when the flange thickness is less than 14 mm, the finite element calculation results are slightly larger than the simplified calculation results. The above calculation method provides methodological support for the simplified calculation of engineering design.

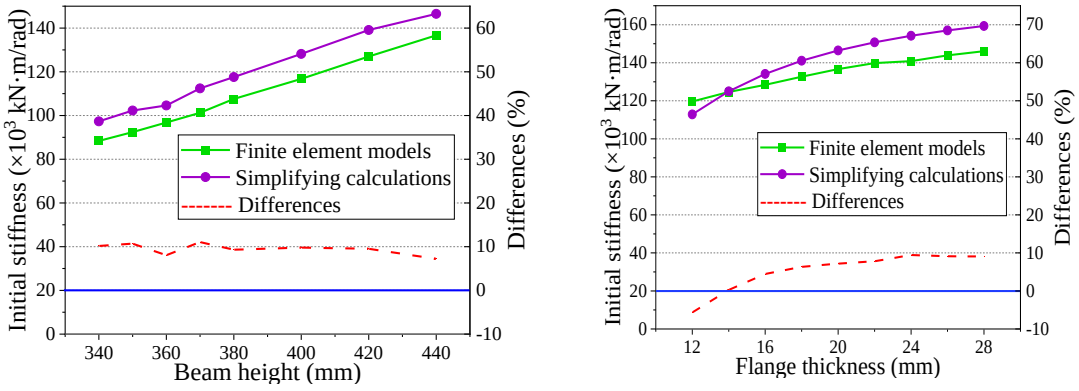


(a) Different beam heights

(b) Different flange thicknesses

**Fig. 37** Comparison of initial stiffness of different methods

## 8. Conclusion

The study delved into the mechanical properties of a novel prefabricated column-beam-column joint using finite element analysis and presented a simplified calculation method. The key conclusions are as follows:

(1) The novel prefabricated joints (NPJs) can accommodate beams of different heights, offering advantages such as convenient construction, controllable quality, reasonable force transfer path, and ease of disassembly and replacement. The validity of the finite element models and simulation parameters was verified through comparison with experimental data.

(2) Under static force at the beam end, the NPJs exhibit a failure mode of beam bending-shear yielding and upper flange bolt failure. In comparison to traditional welded joints, NPJs show slightly smaller plastic moment and ultimate moment by 0.87% and 16.08%, respectively, but possess 16.08% larger initial stiffness. This indicates good static properties and increased construction efficiency.

(3) Hysteresis analysis demonstrates that NPJs have robust load capacity under positive and negative bending moments, with full hysteresis curves. While NPJs exhibit lower ductility coefficient and energy dissipation coefficient than welded joints, both types meet code requirements and demonstrate good seismic performance.

(4) Parametric analysis reveals that the thickness of the flange plate significantly impacts initial stiffness and damage mode, while the number of flange bolts on the beam has a minor effect on static performance. Additionally, an increase in lug plate thickness enhances the joint's mechanical properties during initial loading, and the height of the beam is a crucial factor affecting load carrying capacity.

(5) The study provides and verifies methods for calculating the load carrying capacity and initial stiffness of the novel joint based on design codes GB50017 and Eurocode 3, respectively. These simplified calculation methods empower engineers to design suitable prefabricated steel frame joints effectively.

These conclusions not only contribute to the understanding of the mechanical behavior of novel prefabricated joints but also offer practical insights for designing and implementing such joints in construction projects.

## Acknowledgment

This work was financially supported by the General Program of Science Foundation of Shandong Province (ZR2023ME215), the National Natural Science Foundation of China (Grant No. 52308161 and Grant No. 51308154) and Technology research project of CSCEC (CSCEC-2020-Z-35).

## References

[1] Peng Z, Wang Y, Zhang M W. Mechanics property analysis of prefabricated rectangular steel tube and H-steel-beam connection joint[J]. Journal of Qingdao University of Technology, 2016.

[2] Li G, Zhang J, Li L, et al. Progressive Collapse Resistance of Steel Framed Buildings Under Extreme Events[J]. Advanced Steel Construction, 2021, 17: 318-330.

[3] Taheripour M, Hatami F, Raoufi R. Numerical Study of Two Novel Connections with Short End I or H Stub in Steel Structures[J]. Advanced Steel Construction, 2022, 18: 495-505.

[4] Ma C, Li G, Wang Z. Experimental Study on Mechanical Performance of Buckling-Restrained Brace on Frames with High-Strength Concrete-Filled Square Steel Tube Columns[J]. Advanced Steel Construction, 2023, 19: 293-307.

[5] Zhang Y, Li D. Development and testing of precast concrete-filled square steel tube column-to-RC beam connections under cyclic loading[J].Construction and Building Materials, 2021, 280:122540.

[6] Torabian S, Mirghaderi S R, Keshavarzi F. Moment-connection between I-beam and built-up square column by a diagonal through plate[J].Journal of Constructional Steel Research,2012,70(2):385-401.

[7] Hassan M K, Tao Z, Katwal U. Behaviour of through plate connections to concrete-filled stainless steel columns[J]. Journal of Constructional Steel Research, 2020, 171.

[8] Lai-Yun W, Lap-Loi C, Sheng-Fu T. Seismic behavior of bolted beam-to-column connections for concrete filled steel tube. Journal of Constructional Steel Research, 2005(61):1387-1410.

[9] Wang X, Hao J, Pan Y, et al. Behavior research of through high strength bolts-end plate connection for concrete filled square steel tube column. Industrial Construction 2008, 38(3): 23-26. (in Chinese)

[10] Zong Z, Lin Y, Lin J. Experimental study on seismic performance of rectangular concrete-filled steel tube column-to-steel beam semi-rigid connections. Journal of Building Structure 2004, 25(6): 29-36. ( in Chinese)

[11] Sun J, Qiu H, Xu J. Experimental Verification of Vertical Joints in an Innovative Prefabricated Structural Wall System. Advances in Structural Engineering. 2015, 18(7):1071-1086.

[12] Zaid A, Moussa L, Ahmed F. Experimental validation of a novel curved steel damper for steel frames with flexible beam-column joints[J]. Structures, 2023, 56:105010.

[13] Shakeri J , Abdollahzadeh G .Seismic Rehabilitation of Tall Steel Moment Resisting Frames Damaged by Fire with SMA-Based Hybrid Friction Damper[J]. International journal of steel structures, 2020(1):20.

[14] Reza S, Farhad B.Experimental Studies on a Combined Damper for Repairable Steel Moment Connections[J]. International Journal of Steel Structures, 2018(18): 211-2224.

[15] Hongkai D, Pengfei Z, Yuandong W, et al. Seismic experimental assessment of beam-through beam-column connections for modular prefabricated steel moment frames[J]. Journal of Constructional Steel Research, 2022, 192: 107208.

[16] Ozkula G. High strength steel for seismic resistance of beam-to-column connections： novel metal investigation[Z]. 2011.

[17] Cui Y,Luo Y,Nakashima M. Development of steel beam-to-column connections using SFRCC slabs[J]. Engineering Structures,2013,52：545-557.

[18] Farmani M A,Ghassemieh M. Steel beam-to-column connections equipped with SMA tendons and energy dissipating devices including shear tabs or web hourglass pins.[J]. Journal of Constructional Steel Research, 2017, 135：30-48.

[19] Ataei A, Valipour H R, Bradford M A, et al. Experimental study of steel-timber composite beam-to-column joints with extended end plates[J]. Construction and Building Materials, 2019, 226:636-650.

[20] Chen H, Ke C, Chen C, et al. The Tensile Performance of Inter-Module Connection with a Bolt and Shear Key Fitting for Modular Steel Buildings[J]. Advanced Steel Construction, 2023, 102-111.

[21] Cheng M, Zhang Y, Li Z, et al. Experimental Study of Hysteretic Behavior of Resilient Prefabricated Steel Frames with and without Intermediate Columns[J]. Advanced Steel Construction, 2022, 18: 715-727.

[22] Kristóf I,Novák Z,Hegyi D. A Simplified Method for the Design of Steel Beam-to-column Connections.[J]. Periodica Polytechnica： Architecture, 2017, 48(2): 79-86.

[23] Liu X C, Yang Z W, Wang H X, et al. Seismic performance of H-section beam to HSS column connection in prefabricated structures[J]. Journal of Constructional Steel Research, 2017,138:1-16.

[24] Zhiwei Z, Huajie W, Hongliang Q, et al. Design and Mechanical Performance Analysis of a New Type of Column-Column-Beam Prefabricated Steel Frame Joint[J]. Structural Engineering International, 2021, 31(3).

[25] Wihlborg A, Crafoord R. Steel sheet surface topography and its influence on friction in a bending under tension friction test[J]. International Journal of Machine Tools & Manufacture, 2001, 41(13):1953-1959.

[26] GB50017-2017. Code for Design of Steel structures, 2017. (in Chinese)

[27] Bi Y. Study on mechanical properties of assembled joints between high square steel tube columns and H-shaped steel beams with adjustable beams [D]. Harbin Institute of Technology, 2019. (in Chinese)

[28] Huajie W, Borui Z, Hongliang Q, et al. Experimental and numerical studies of a new prefabricated steel frame joint without field-welding: Design and static performance - ScienceDirect[J]. Thin-Walled Structures, 2020, 159.

[29] EN 1993-4-3:2007, Eurocode 3- Design of steel structure, 2007.